2009 IEEE/ASME International Conference on Advanced Intelligent Mechatronics
Suntec Convention and Exhibition Center
Singapore, July 14-17, 2009

Intelligent Equivalent Physical Simulator for Nanosatellite Space Radiator

Yun-Ze Li, *Member, IEEE,* Kok-Meng Lee, *Fellow, IEEE/ASME*, and Jun Wang

Abstract— Experimental prediction of the in-orbit transient performance of a nanosatellite space radiator requires a ground-based equivalent space radiator capable of high precision simulation under a wide range of various working conditions. This paper presents the working principle and the fuzzy control algorithm of a novel intelligent equivalent physical simulator (EPS) consisting of a thermoelectric cooler (TEC), a plate-fin heat sink and a forced cooling fan and a integrated fuzzy controller. The TEC-based IEPS achieves the purpose of simulating the in-orbit transient heat radiation in an earth atmospheric environment by adapting two key parameters: the TEC cooling capacity, and the thermal resistance of the heat-sink cooling fan. This paper offers the design and evaluation of a fuzzy controller for the IEPS as an attractive alternative to the traditional PID controller. The fuzzy control presented here will have other potential thermal control applications where TECs and forced cooling heat sinks are employed.

Index Terms—Nanosatellite, space radiator, ground-based physical simulation, thermoelectric cooler, fuzzy control.

I. Introduction

Recent advances in MEMS fabrication technology have resulted in a number of emerging mechatronics. Among them are nanosatellites (each with a wet mass between 1 and 10 kg or 2.2–22 lb), which have the potential of revolutionizing the space industry and can help achieve ambitious missions such as inter-spacecraft communications [1] and earth observation [2]. Space radiators play an important role in dissipating heat generated inside the satellite to the space environment [3], and this transfer process is dominated by the heat radiation at the radiator surface [4]-[7]. Because of its large power density, small thermal capacity and small available surface area for radiation, nanosatellites are subject to relatively stiff heat dissipating task. The impacts of external heat flux (such as direct solar radiation, earth infrared radiation and earth reflected solar radiation) on the transient thermal response of the radiators and on the internal temperature dynamics of the nanosatellite are much higher than that of large ones. These, combined with highly integrated systems that dissipate large amounts of power in a small volume, demand careful design of the thermal control system in order to meet stringent temperature control requirements.

Manuscript received January 26, 2009. This work was supported by the National Natural Science Foundation of China, the Aeronautic Science Foundation of China and the Lantian-xinxing Program for Excellent Talents in Beihang University under Grants 50506003, 2008ZC51028, and 2007221237 respectively. It was partly carried out during Yun-Ze Li's stay at Georgia Institute of Technology.

Y.-Z. Li and J. Wang are with the School of Aeronautic Science and Engineering, Beihang University, Beijing 100191, China (e-mail: liyunze@ buaa.edu.cn ; wangjun@ buaa.edu.cn).

K.-M. Lee is with The George W. Woodruff School of Mechanical Engineering, Georgia Institute of Technology, Atlanta, GA 30332-0405, USA(e-mail: kokmeng.lee@me.gatech.edu).

Since the ground based experiments are the primary ways to investigate satellites' in-orbit performance before launched, the space simulator become an essential tool for predicting the thermal behaviors of the satellite surfaces which include radiators [8]. A typical space simulator usually consists of a vacuum chamber, heat sink, cryogenic subsystem, heating subsystem and vacuum pumping subsystem [9]-[11]. This ground-based physical simulation approach has been widely used in the thermal cycling, vacuum and balance tests [12]-[14] for a satellite. However, these traditional space simulators are too large, complex and slow for investigating the dynamics of the internal thermal control loop strategies of the nanosatellite or the effects of active thermal control, where critical response time requirements must be met.

A smaller and simpler (but with a faster response) ground-based physical apparatus, referred to here as an *equivalent physical simulator (EPS)*, is required as a rational basis for simulating the nanosatellite space radiator and for investigating the dynamic performance of its internal thermal control system. Thermoelectric coolers (TECs), which are much more compact than other kinds of refrigerators, are among the best candidates for the EPS, because of their small size, low thermal inertia, fast dynamic response and easy of control. Although the TEC has been widely employed in the thermal management of electronic systems where extremely stable temperature control is required, most of the studies have largely focused on the design, analysis and experiment of thermoelectric elements [15]-[20]. Due to the highly non-linear dynamic behavior of the thermoelectric module [21], it is very difficult to model its transient performance accurately with theoretical equations; thus, a linear approximation is often rendered to simplify it for control system design. A practical alternative to this perturbation control system analysis is the employment of fuzzy logics, which has shown some potential to improve the control effect of thermoelectric system [22]. Similar improvements can also be found in other fuzzy applications like robotic tracking of moving objects [23], robot navigation [24], gas turbine control [25], and more recently mechatronic system modeling [26]. However, unlike the traditional TEC applications where the cold–side temperature is usually the only controlled variable and is always lower than the surrounding temperature [15]-[22], the desired cold-side working temperature of the TEC for the ground-based space radiator EPS may be *higher than*, *lower than* or *equal to* the atmosphere temperature. In addition, the cooling heat flux and cold-side temperature of the TEC during the transient in earth convection environment must be controlled with high precision

978-1-4244-2853-3/09/$25.00 ©2009 IEEE

to simulate those of the space radiation heat transfer. These differences demand advanced intelligent control strategies to meet the stringent requirements including a wide working range and high simulating precision of the ground-based EPS.

The remainder of this paper offers the followings:

- We present the working principle, dynamical model of a novel intelligent equivalent physical simulator (EPS) developed for a nanosatellite space radiator (nS-SR). The intelligent EPS consisting of a TEC and a fan/sink cooling system simulates the heat dissipating effect of the nS-SR by adjusting the TEC cooling capacity under intelligent fuzzy control. The TEC-based EPS is conveniently small and structurally simple but sufficiently fast in dynamic response for ground-based experimental investigation of the transient performance impact on the internal thermal control system of the nS-SR being tested.
- We offer an intelligent fuzzy control approach for controlling the TEC and its hot-side working temperature, and numerically evaluate its control performances (subject to step disturbances due to thermal load changes and air temperature variation) against those under traditional PID control. As will be shown, the response of the fuzzy controlled EPS agrees well with that of the simulated nS-SR. In addition, it offers a faster response and exhibits a smaller overshoot than that under PID control.

II. Principle, Configuration and Dynamical Equations of EPS

The function of a nanosatellite space radiator (nS-SR) is to dissipate heat generated inside the satellite to the space environment as shown in Fig. 1 where T_r is the temperature at the radiator surface (with area A). When flying in the low earth orbit, the nS alternates between in the shadow of the earth and in the direct exposure of sunlight. In orbit, the transfer process at the outer surface of the nS-SR is dominated by the heat radiation (Fig. 1a) with the net radiant heat flux given by

$$Q_r = \varepsilon\sigma A T_r^4 - A\sum_{i=1}^{3}\alpha_i q_i \quad (1)$$

where σ is the Stefan-Boltzmann constant; ε is the radiator surface emittance; α_i and q_i are the radiator absorptions and radiant heat flux density at the outer surface respectively; and the subscripts, i=1, 2, and 3, denote the contributions from the solar radiation, earth radiation, and albedo (or the earth surface reflectivity of sun radiation) respectively.

Before the nanosatellite is launched into its orbit, the heat dissipation is governed by heat convection between the radiator and the earth's atmosphere (Fig.1b) with the net convective heat flux expressed as

$$Q_r = Q_{er} - h_r A(T_r - T_a) \quad (2)$$

where Q_{er} is total external radiation heat flux absorbed by the simulated nS-SR; T_a is the atmosphere temperature; and h_r is the heat transfer coefficient.

The need to simulate the space radiation heat transfer (1) under heat transfer mode (2) in earth convection environment, makes it necessary to develop a ground-based simulator that can experimentally investigate the static temperature distribution and transient temperature response of the nanosatellite so that its in-orbit thermal control effects are well understood, especially during the design and development phase, and the evaluation testing stage of a new satellite.

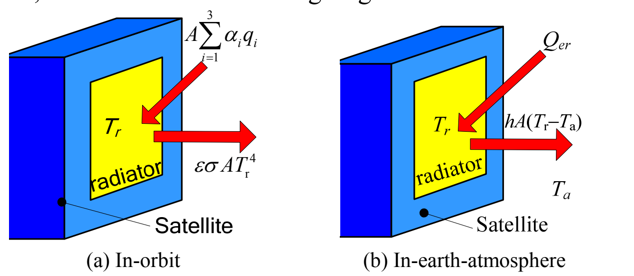

Fig.1 Heat transfer of a nanosatellite space radiator

A. *Equivalent Physical Simulator (EPS) of the nS-SR*

Figure 2 shows the EPS for realistically simulating the thermal behavior of an nS-SR on ground. The primary components of the EPS are the thermoelectric cooler (TEC) and the plate-fin heat sink with the forced cooling fan. A heat flux sensor (denoted as Q_c in Fig. 2) is mounted on the cold-side of the TEC while temperature sensors are placed on both hot- and cold-sides of the TEC, which are denoted in Fig. 2 as T_h and T_c respectively. When the EPS is employed for ground-based experiments, the cold-side of the TEC is attached to the nS-SR surface. As shown in Fig. 2, the other surfaces of the nanosatellite are covered with thermal insulation so that the influence of earth atmosphere to their thermal states can be minimized. Electric heating elements are placed on the inside of this thermal insulation layer to control the thermal load Q_i, and hence simulate the surface temperature of the tested nS-SR.

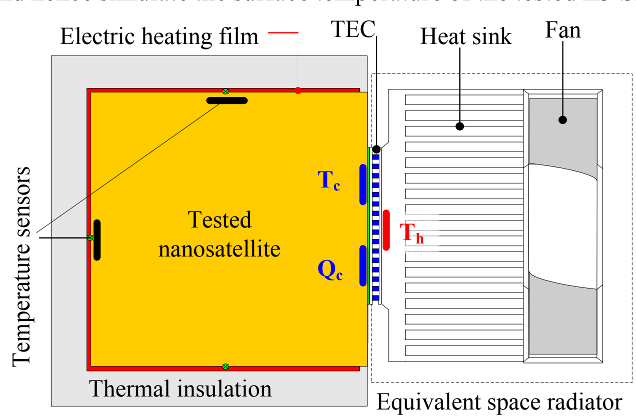

Fig. 2 Equivalent Physical Simulator (EPS)

In operation, the electric current input to the TEC is adjusted according to the cooling heat flux and temperature at the cold side of the TEC to simulate the cooling effect of the nS-SR equivalently. Since the *real* temperature T_r (of the nS-SR being simulated) may be higher or lower than the earth atmosphere temperature T_a, a flexible controller for the hot-side temperature T_h must be designed so that both cold-case ($T_r < T_a$) and hot-case ($T_r \geq T_a$) can be simulated. This means that the thermal resistance of the heat sink must be adjusted according to the cold-side temperature T_c. This is realized by manipulating the electric current that drives the forced cooling fan.

B. Principle and Dynamical Equations

To illustrate the operational principle, we treat the cold-side of the TEC as a lumped-parameter node in modeling the EPS dynamics:

$$\left(V_{c}\rho_{c}c_{c}\right)\dot{T}_{c} = Q_{i} - Q_{c} \tag{3}$$

where (V_c, ρ_c, c_c) are the volume, average density and specific heat of the TEC; T_c and Q_i are the temperature and the thermal load at the cold-side of TEC; and Q_c is the TEC cooling capacity. The theoretical cooling capacity of the TEC for a specified electric current I_t passing through it is given by (3a):

$$Q_{c} = \alpha_{t}T_{c}I_{t} - RI_{t}^{2}/2 - K\left(T_{h} - T_{c}\right) \tag{3a}$$

where α_t, R and K are the Seeback coefficient, electrical resistance, and thermal conductivity of the TEC respectively; and T_h is the hot-side temperature of the TEC.

In order to simulate the in-orbit thermal behavior of the nS-SR equivalently using the TEC, the cooling capacity Q_c and the cold-side temperature T_c of the TEC should be equal to the net radiant heat flux Q_r and the working temperature T_r of the nS-SR respectively; in other words,

$$Q_{c} \to Q_{r} \text{ at } T_{c} \to T_{r} = \text{specified working temperature} \tag{3b}$$

The desired condition (3b) is accomplished by adjusting the electric current I_t of the TEC to reach the equivalent cooling effect. Since (3a) and (3b) must be met simultaneously, the electric current to drive the TEC for simulating the in-orbit heat radiation can be found by equating them:

$$I_{t} = \frac{1}{R}\left(\alpha_{t}T_{c} \pm \sqrt{\alpha_{t}^{2}T_{c}^{2} - 2RQ_{e}}\right) \tag{4}$$

where $$Q_{e} = \varepsilon\sigma A T_{c}^{4} - A\sum_{i=1}^{3}\alpha_{i}q_{i} + K(T_{h} - T_{c}) \tag{4a}$$

The lower value of the solution of (4) is preferred to reduce the TEC power consumption P which is given by

$$P = \alpha_{t}(T_{h} - T_{c})I_{t} + I_{t}^{2}R \tag{5}$$

Similarly, we treat the TEC hot-side and the heat-sink together as another lumped-parameter node, and neglect the small thermal resistance between the TEC and the heat sink. The total heat flux Q_h (including Q_c and that generated from the TEC) reaching the hot-side of the TEC must be rejected to the earth atmosphere (at temperature T_a) through the heat sink. The cooling fan offers a means to manipulate the thermal resistance R_h between the hot-side of the TEC and earth atmosphere by adjusting its electric current I_f. Thus, the EPS dynamics at the hot-side is given by (6):

$$\left(V_{h}\rho_{h}c_{h}\right)\dot{T}_{h} = Q_{h} - \left(T_{h} - T_{a}\right)/R_{h} \tag{6}$$

where (V_h, ρ_h, c_h) are the volume, density and specific heat of the heat sink. The heat flux Q_h (=Q_c+P) pumped to the TEC hot-side can be calculated from:

$$Q_{h} = \alpha_{t}T_{h}I_{t} + RI_{t}^{2}/2 - K(T_{h} - T_{c}) \tag{6a}$$

The desired thermal resistance R_h of the heat sink, which is defined in (6b), is determined from the forced convection at the heat-sink surface:

$$R_{h} = \frac{T_{h} - T_{a}}{Q_{h}} = \left(\frac{1}{\dot{m}c_{pa}}\right)\frac{\exp(\gamma)}{\exp(\gamma) - 1} \quad \text{where } \gamma = \eta\frac{h_{h}A_{h}}{\dot{m}c_{pa}} \tag{6b}$$

where γ is the number of transfer units of the heat sink; ($\dot{m}$, c_{pa}) are the mass flow rate and specific heat of the forced cooling air; (η, A_h) are the fin efficiency and heat transfer area of the heat sink; and h_h is the convective heat transfer coefficient between the heat sink surface and air.

Given the cooling capacity Q_c in (3a) and power supply P in (5), the TEC performance can be evaluated using the parameter coefficient of performance (COP) defined in (7):

$$COP = Q_{c}/P \tag{7}$$

A high COP means less power consumed by the TEC, the key component in simulating the nS-SR.

III. Intelligent Control Strategies and Numerical Investigation Results

The TEC as well as the forced cooling fan with heat sink of the EPS are typical nonlinear controlled systems. There are difficulties in reducing their nonlinear constitutive equations to simple linear models and yet accurately and conveniently reflecting their dynamics [19]. Also, there are challenges of experimentally identifying the parameters that characterize the linear dynamical model at various working conditions [21]. To overcome these difficulties, we explore here a fuzzy control algorithm as an effective alternative to traditional control methods [22] [23].

A. Operating Patten and Strategies

The two following case-operations are required of the TEC-based EPS simulation:

Cold-case ($T_r < T_a$) and *hot-case* ($T_r \geq T_a$)

However, for equivalent-ground-based experiments, the TEC hot-side temperature T_h must be higher than earth atmosphere temperature T_a to allow for heat dissipation, and as low as possible for economical operation of the TEC. To accommodate these requirements, the hot-side temperature T_h of the TEC is adapted using the control strategy (8):

$$T_{h} = \begin{cases} T_{a} + \delta_{c} & \text{if } T_{r} < T_{a} \text{ (cold-case)} \\ T_{c} + \delta_{h} & \text{if } T_{r} \geq T_{a} \text{ (hot-case)} \end{cases} \tag{8}$$

where δ_c and δ_h are small positive constants for efficient operation of the TEC and the ease of control of the cooling fan. This can be realized by adjusting the electric current of the cooling fan. The results are illustrated in Fig. 3 showing the desired variation in the thermal resistance R_h, and the corresponding hot-side dissipated heat Q_h and temperature T_h as a function of the cooling air velocity v_s.

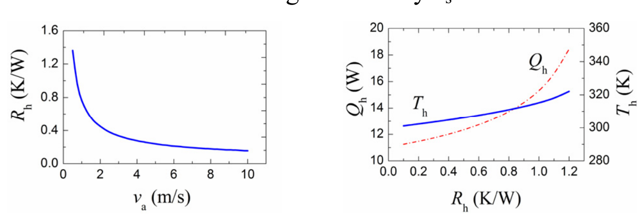

(a) Thermal resistance changes with the velocity of cooling air

(b) Effect of thermal resistance variation

Fig. 3 Variation of hot-side thermal resistance and its effects

B. Intelligent Controller

Figures 4(a) and 4(b) show the block diagram illustrating the EPS control system and the fuzzy logic controller. The hardware implementing the intelligent controller is illustrated in Fig. 4(c), where two sensors measuring T_c and heat flux Q_c are mounted on the cold-side, and another temperature sensor is placed on the hot-side of the TEC. The sensing signals are fed to the integrated control unit as inputs. The control unit outputs two signals manipulating the electric currents that drive the TEC and the cooling fan of the heat sink.

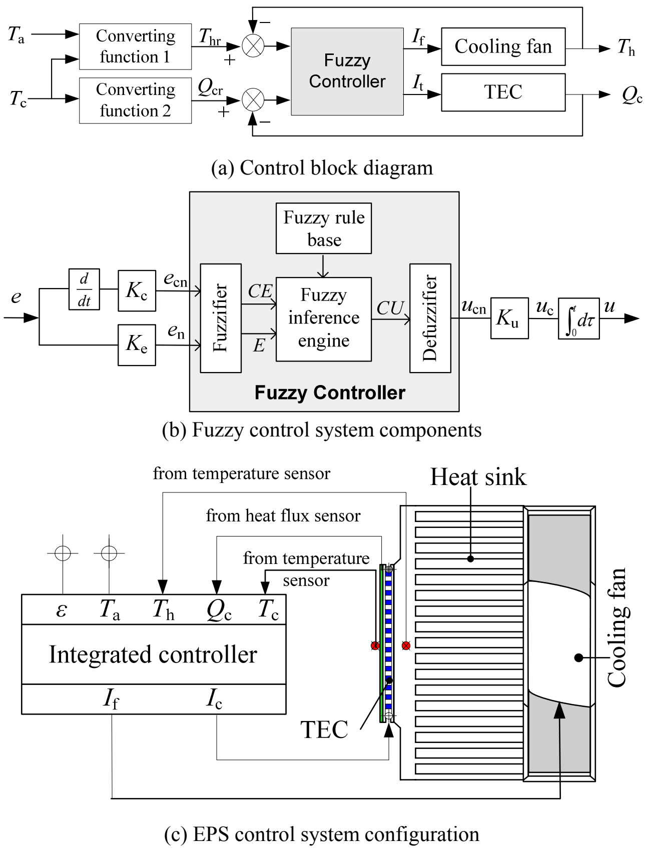

Fig. 4 Block diagrams illustrating the EPS controller

As shown in Fig. 4(a), the cold-side cooling heat flux Q_c and the hot-side temperature T_h are manipulated through the electrical currents (I_t and I_f) to the TEC and the cooling fan respectively. The corresponding reference values are given by the following converting functions:

$$Q_{cr} = \varepsilon\sigma A T_c^4 - Q_{er} \tag{9}$$

and

$$T_{hr} = \max(T_c, T_a) + \delta \tag{10}$$

where Q_{er} is the total external space heat flux absorbed by the simulated nS-SR. In (10), δ is small constant (usually about 1 to 5K) and is added to maintain a positive (T_h–T_a) under the cold-case or a positive (T_h–T_c) under the hot-case so that heat can be transferred out of the heat-sink or the TEC respectively.

Figure 4(b) shows the fuzzy incremental controller consisting of a fuzzifier, an inference engine, a defuzzifier and a fuzzy rule-base. The inputs to the fuzzifier are the error e_n and its difference e_{cn} normalized by the factors K_e and K_c. Similarly, the output u_{cn} (scaled by the factor K_u) leaving the defuzzifier is a normalized increment of the controlling variable u (I_f or I_c). The input and output variables to the fuzzy controller are characterized by the fuzzy sets, linguistic values and associated analytical ranks in Table 1. Each fuzzy set (or its linguistic value) is defined by a Gaussian membership function shown in Fig. 5. The membership functions have an overlap with each other in order to provide a smooth output transition between regions.

The controller output is determined from the linguistic rules in the following form:

IF e_n is E_i and e_{cn} is CE_j, THEN u_{cn} is $CU_{k(i,j)}$

where E_i and CE_j and $CU_{k(i,j)}$ are the fuzzy values of e_n, e_{cn} and u_{cn}; and the subscript variables *i*, *j*, and *k(i,j)* denote the analytical ranks associated with these linguistic values in Table 2. For a two-input system (e_n and e_{cn}, each with nine fuzzy values), a fully populated rule base will have 9×9=81 input rule combinations derived with the aid of simulations, which suggest the following:

– A positive error e_n can be effectively reduced by a positive input increment to TEC but a negative input increment to the cooling fan.
– When the error e_n is positively large but its difference e_{cn} is negatively large, the input increments to TEC should be zero or negatively low (while to the cooling fan should be zero or positively low) because a reverse error change rate can effectively reduce the control output changes in order to achieve a better result.
– Similarly, when e_n is negatively large but e_{cn} is positively large, the input increments to TEC should be zero or positively low, and that to the cooling fan should be zero or negatively low.

TABLE 1: FUZZY SETS AND THEIR LINGUISTIC VALUES

Fuzzy sets	Ranks	Linguistic values	Fuzzy sets	Ranks	Linguistic values
NS	–4	negative super	PS	4	positive super
NH	–3	negative high	PH	3	positive high
NM	–2	negative medium	PM	2	positive medium
NL	–1	negative low	PL	1	positive low
ZE	0	zero			

* Associated ranks are for the convenience of rules producing.

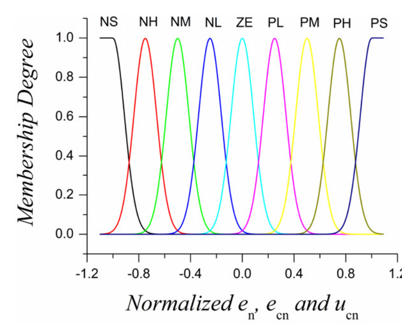

Fig. 5 Membership functions

On the basis of these insights, the rank-based rule generating policy is derived in (11):

$$k(i,j) = \begin{cases} +[\varphi i + (1-\varphi) j] & \text{TEC control} \\ -[\varphi i + (1-\varphi) j] & \text{Fan control} \end{cases} \tag{11}$$

where φ is the error impact power determined by the rank of the input error. Here the same parameter producing law is used for both TEC control and its fan control:

$$\varphi = 0.8 - 0.1|i| \quad \text{where } 0 \le i \le 4 \tag{12}$$

Fuzzy control rules produced by (11) and (12) for the intelligent control of the TEC and heat-sink cooling fan are plotted in Fig.6, which are rounded off to integer ranks for characterizing into a 9-element fuzzy set {NS, NH, NM, NL, ZE, PL, PM, PH, PS}. As the control rules (Fig. 6b) for the cooling fan are complements of those for the TEC (Fig. 6a), only the fuzzy control rules of the TEC intelligent controller are summarized up in Table 2.

In Fig. 4(b), the output from the defuzzifier takes the form:

$$u_{\mathrm{cn}} = \sum_{i=1}^{9}\sum_{j=1}^{9} u_{\mathrm{cn},k,}\lambda_{k(i,j)} \Bigg/ \left(\sum_{i=1}^{9}\sum_{j=1}^{9}\lambda_{k(i,j)}\right) \qquad (13)$$

where $u_{\mathrm{cn},k}$ and $\lambda_{k(i,j)}$ are the representative discrete element and membership degree of the output fuzzy set $CU_{k(i,j)}$. The next control step u' can then be determined in terms of the current control step u and u_{cn} by (14):

$$u' = u + K_{\mathrm{u}} u_{\mathrm{cn}} \quad \text{where } u \in \{I_{\mathrm{t}}, I_{\mathrm{f}}\} \qquad (14)$$

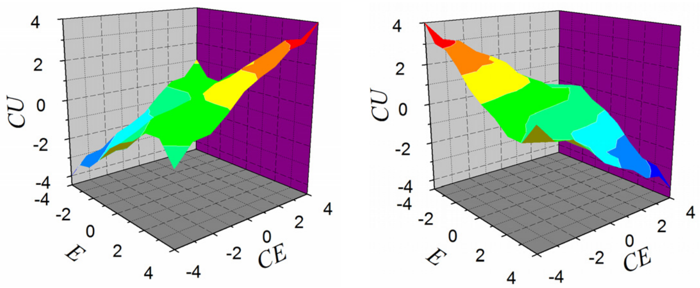

(a) TEC control (b) Forced cooling fan control

Fig. 6 Surface map of the fuzzy control rule base

TABLE 2: FUZZY CONTROL RULES OF TEC

E_i/CE_i	NS	NH	NM	NL	ZE	PL	PM	PH	PS
NS	NS	NH	NH	NM	NM	NL	ZE	ZE	PL
NH	NH	NH	NM	NM	NL	NL	ZE	ZE	ZE
NM	NH	NM	NM	NM	NL	NL	ZE	ZE	ZE
NL	NM	NM	NL	NL	NL	ZE	ZE	ZE	PL
ZE	NL	NL	ZE	ZE	ZE	ZE	ZE	PL	PL
PL	NL	ZE	ZE	ZE	PL	PL	PL	PM	PM
PM	ZE	ZE	ZE	PL	PL	PM	PM	PM	PH
PH	ZE	ZE	ZE	PL	PL	PM	PM	PH	PH
PS	NL	ZE	ZE	PL	PM	PM	PH	PH	PS

C. Simulation of the Dynamics and Control

To examine the effectiveness of the fuzzy controlled intelligent EPS under different working conditions, we predict its dynamics subject to disturbances due to

- a −5K step change in the atmosphere temperature T_{a}.
- a +10% step change in the input thermal load Q_{i} and

As a basis for evaluation, we compare the predictions against simulations of a PID controlled EPS system (with parameters K_{p}, $K_{\mathrm{p}}/T_{\mathrm{i}}$, $K_{\mathrm{p}}T_{\mathrm{d}}/T_{\mathrm{s}}$, where K_{p} is a proportional gain; T_{i} and T_{d} are the integral and derivative times in seconds respectively; and T_{s} is the sampling period). The parameter values of the controllers and their controlled EPS used in the simulation are summarized in Table 3 and Table 4.

TABLE 3: PARAMETERS OF SIMULATED CONTROLLERS

Fuzzy controller			PID controller		
Parameters	TEC	Fan	Parameters	TEC	Fan
K_{e}	0.05	0.01	K_{p}	0.055	−0.05
K_{c}	0.05	0.01	T_{i}	10	15
K_{u}	1.0	1.0	T_{d}	0.05	0
Sampling period, T_{s}=1.0 second					

The effectiveness of the fuzzy controller (Fig. 4) along with the T_{h} adaptation strategy (10) can be observed from the simulated transient responses of the cold- and hot-side temperatures (T_{c} and T_{h}) given in Figs.7, 8 and 9:

- As shown in Fig 7(a), in response to the −5K step change in the surrounding atmosphere, T_{r} remains unchanged as expected in (1) since there is no change in the input cooling load and in obit, T_{a} does not affect the simulated nS-SR temperature; T_{c} fluctuates within 2% of its steady state value (the absolute overshoot is only 0.25K and agrees with T_{r} well). The effect of the −5K step change in T_{a} can be seen in Fig 7(b) to be primarily taken on by T_{h} during this transient, which returns to its steady state value after a few oscillations (but no more than ±2K).

TABLE 4: VALUES OF EPS PARAMETERS

Parameter (Unit)	Symbol	Value
Design specification		
Cooling capacity (W)	Q_{c}	10
Cold-side temperature (K)	T_{c}	300
Atmospheric temperature (K)	T_{a}	298.15 (25°C)
TEC parameters		
Seeback coefficient (W/K/A)	α_{t}	0.051
Electrical resistance (Ω)	R	2.22
Thermal conductivity (K/W)	K	0.5808
Specific heat (kg/m^3)	ρ_{c}	2420
Average density (kJ/kg)	c_{c}	0.713
Geometrical dimension (mm)	$H{\times}L{\times}W$	4.5×40×40
Plate-fin Heat Sink		
Device dimension (mm)	$H{\times}L{\times}W$	34×82×67.5
Specific heat (kg/m^3)	ρ_{h}	2610
Average density (kJ/kg)	c_{h}	0.904

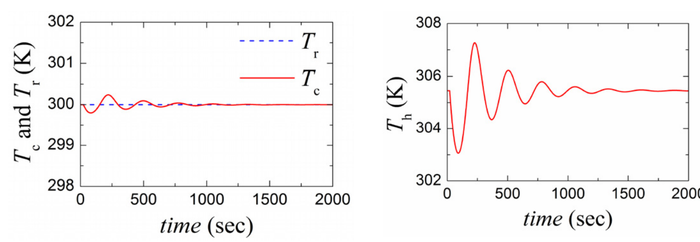

(a) Cold-side temperature (b) Hot-side temperature

Fig. 7 Effect of −5K change in T_{a} on fuzzy controlled EPS

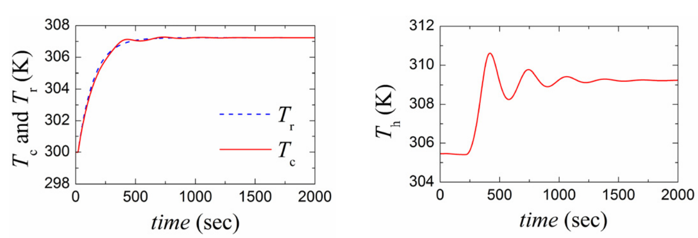

(a) Cold-side temperature (b) Hot-side temperature

Fig. 8 Effect of +10% step change in Q_{i} on fuzzy controlled EPS

- Figure 8(a) compares the transient responses of the cold-side temperature T_{c} and the simulated nS-SR temperature T_{r} to a +10% change in Q_{i}. The simulation shows that T_{c} and T_{r} settle to the new steady state value of 307 K in approximately 320 seconds with little or no significant overshoot. The transient responses of T_{c} and T_{r} closely agree with each other; the dynamic tracking errors of T_c with respect to T_r is less than 0.25 K. The corresponding transient response of the hot-side temperature T_h is given in Fig. 8(b). Unlike the cold side temperature, T_h exhibits a 35% overshoot (about 1.4 K) and a pure time delay 230 seconds because of the thermal inertia of heat sink as shown in (3). This overshoot and delay, however, are acceptable since they do not affect the T_c response.

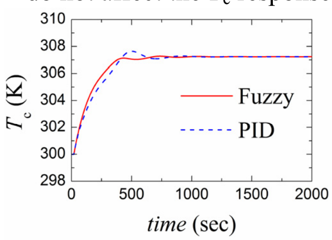

(a) Cold-side temperature

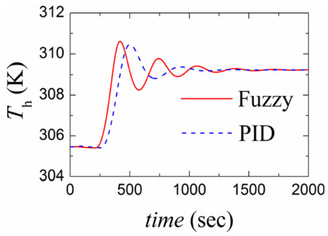

(b) Hot-side temperature

Fig.9 Comparison between Fuzzy and PID EPS control (+10% change in Q_i)

- As compared in Fig.9, the fuzzy controlled T_c and T_r are more responsive and with a smaller overshoot than that of a PID control when experiencing a +10% step change in Q_i.

IV. Conclusion

We have presented the working principle, operating strategies, and fuzzy control algorithm of a ground-based EPS for simulating the transient heat radiation of an in-orbit nS-SR in an earth atmospheric environment. In addition, we present the design of the fuzzy controlled EPS and evaluate its performance by comparing the transient temperature responses of the ground-based EPS and the real in-obit nS-SR to a step change in thermal load. The results demonstrate that the fuzzy controller with the method of hot-side temperature adaptation is an attractive alternative to the traditional PID controller. While the intelligent fuzzy-logic control method offered here has been illustrated in the context of a simple and intelligent EPS (that greatly facilitates the testing of nanosatellites before launched), it is expected that the method will have potential applications in other thermal control systems where TECs and forced cooling heat sinks are employed.

References

[1] P. V. Panetta, "NASA-GSFC nano-satellite technology development," *AIAA/USU Conf. on Small Satellites*, Paper No. SSC98-VI-5, pp 1-17.

[2] J. Esper, P. V. Panetta, M. Ryschkewithsch, W. Wiscombe, S. Neeck, "NASA-GSFC nano-satellite technology for earth science missions," *Acta Astronaut.*, Vol. 46, no. 2-6, pp. 287-296, Feb. 2000.

[3] V. Baturkin, "Micro-satellites thermal control concept and components," *Acta Astronaut.*, Vol. 56, no. 1-2, pp. 161-170, Jan. 2005.

[4] R. Osiander, S. L. Firebaugh, J. L Champion, D. Farrar, M. A. G. Darrin, "Microelectromechanical devices for satellite thermal control," *IEEE J. Sensors,* Vol. 4, no. 4, pp. 525-531, Aug. 2004.

[5] W. Biter, S. Hess, O. Sung, D. Douglas, and T. Swanson, "Electrostatic radiator for satellite temperature control," *IEEE Aerospace Conf.*, 2005, pp. 781-790.

[6] D. Farrar, W. Schneider, R. Osiander, J. L. Champion, A. G. Darrin, D. Douglas, *et al*, "Controlling Variable Emittance (MEMS) Coatings for space applications," *Intersociety Conf. on Thermal and Thermomechanical Phenomena in Electronic Systems*, pp. 1020-1024.

[7] D. G. Gilmore, *Spacecraft Thermal Control Handbook*, 2nd ed. vol. 1. Segundo, California: The Aerospace Press, 2002, pp. 21-67; 709-757.

[8] R. D. Stark, "Thermal testing of spacecraft," The Aerospace Corp., Los Angeles, CA, Rep. TOR-0172(2441-01)-4, Sep. 1971.

[9] Test Requirements for Launch, Upper Stage, and Space Vehicles, *Department of Defense Handbook*, Vol. 1 and 2, MIL-STD-340A (USAF), Apr. 1999.

[10] Product Verification Requirements for Launch, Upper Stage, and Space Vehicles, *Department of Defense Standard Practice,* MIL-STD-1540D, Jan. 1999.

[11] M. K. Choi, "Thermal design of Landsat-7 ETM Earth/space background simulators," *Proc. IECEC-97 Energy Conversion Engineering Conf.*, (*IECEC-97*) Vol. 2, pp. 1470-1475, Aug. 1997.

[12] R. O. Ambrose, R. S. Askew, "An experimental investigation of actuators for space robots," *Proc. IEEE Int. Conf. Robotics and Automation,* Vol. 3, pp. 2625 – 2630, May 1995.

[13] W. J. Krotiuk, "Engineering testing of the capillary pumped loop thermal control system for the NASA EOS-AM spacecraft," *Proc. IECEC-97,* Vol. 2, pp. 1463-1469, Aug. 1997.

[14] T. W. Kerslake, L. S. Mason, H. J. Strumpf, "High-flux, high-temperature thermal vacuum qualification testing of a solar receiver aperture shield," *Proc. IECEC-97,* Vol. 1, pp. 440-445, Aug. 1997.

[15] D. M. Rowe, *CRC handbook of thermoelectrics,* New York: CRC Press LLC, 1995: Ch. 55.

[16] A. Bejan, *Heat transfer handbook,* Hoboken, New Jersey: John Wiley & Sons, Inc., 2003, pp. 1029-1131.

[17] B. J. Huang, C. J. Chin, C. L. Duang, "A design method of thermoelectric cooler," *Int. J. of Refrigeration*, Vol. 23, pp. 208-218, 2000.

[18] R. Chein and Y. Chen, "Performances of thermoelectric cooler integrated with microchannel heat sinks," *Int. J. of Refrigeration*, vol. 28, pp. 828–839, 2005.

[19] M. Anatone, R. Cipollone, "Theoretical and Experimental Analysis on Thermoelectric Cooling Devices," *J. of Thermophysics and Heat Transfer,* Vol.15 no.4, pp. 447-452, 2001.

[20] L.U. Odhner and H. H. Asada, "Sensorless temperature estimation and control of shape memory alloy actuators using thermoelectric devices," *IEEE/ASME Trans. on Mechatronics.* Vol. 11, issue 2, pp. 139-144, 2006.

[21] B. J. Huang, C. L. Duang, "System dynamic model and temperature control of a thermoelectric cooler," *Int. J. of Refrigeration*, Vol. 23, pp.197-207, 2000.

[22] A. A. Aly, E. A. S. Abo, "Fuzzy temperature control of a thermoelectric Cooler," *IEEE Int. Conf. Industrial Technology*, pp. 1580-1585, Dec. 2006.

[23] K-M. Lee and Y. Qian, "A vision-guided fuzzy logic control system for dynamic pursuit of moving target," *Microprocessor and Microsystems*, Elsevier Science, 1998, 21, pp. 571-580.

[24] X. Chen; K. Watanabe, K. Kiguchi, K. Izumi, "An ART-based fuzzy controller for the adaptive navigation of a quadruped robot," *IEEE/ASME Trans. on Mechatronics,* Vol. 7, Issue 3, pp. 318 – 328, 2002

[25] J-W Kim, S. W. Kim, "Design of incremental fuzzy PI controllers for a gas-turbine plant," *IEEE/ASME Trans. on Mechatronics,* Vol. 8, Issue 3, pp. 410 – 414, 2003.

[26] K. Erenturk, " Hybrid control of a mechatronic system: fuzzy logic and grey system modeling approach," *IEEE/ASME Trans. on Mechatronics*, Vol. 12, Issue 6, pp. 703 – 710, 2007.